fortune Journals

Research Article

CARDIOLOGY AND CARDIOVASCULAR MEDICINE

ISSN: 2572-9292



FOS-Mediated Mitophagy Suppression Links Stress Signaling to Heart Failure Progression

Rui Feng[1*], Meili Liu[1], Zirui Liu[1], Haocheng Wang[1], Danning Cao[1], Jinghui Ai[1], Jikai Wang[1], Weiqi Wang[1], Cao Zou[2*]

Abstract

Heart failure (HF) constitutes the terminal phenotype of cardiovascular disease, defined by profound metabolic disarray and pervasive mitochondrial dysfunction. Contemporary "quadruple therapy" regimens mitigate disease progression primarily through suppression of neuroendocrine activation, yet the fundamental energetic insufficiency that sustains cardiac decline remains unaddressed. Mounting evidence implicates defective mitochondrial autophagy (mitophagy) as a central driver of cardiomyocyte injury. Nonetheless, the upstream transcriptional networks governing the collapse of mitophagy competence remain largely unresolved. To identify molecular determinants of mitophagy impairment in HF, we integrated three independent transcriptomic datasets (GSE95140, GSE133054, GSE141910) using Robust Rank Aggregation with batch correction. Differentially expressed genes (DEGs) were subjected to GO, KEGG, PPI, and GSEA analyses. Hub genes were validated in vivo using a pressure overload–induced transverse aortic constriction (TAC) mouse model and in vitro in primary mouse cardiomyocytes exposed to angiotensin II (Ang II). Functional assays, including echocardiography, histology, qRT-PCR, western blotting, immunofluorescence, and transmission electron microscopy, were employed to assess cardiac remodeling, mitophagy flux, and mitochondrial integrity. Transcriptomic integration revealed 256 consistent DEGs across datasets, primarily enriched in oxidative phosphorylation and mitochondrial metabolic pathways. Protein–protein interaction analysis identified five hub genes FOS, VWF, TAGLN, B2M, and CCL2 with FOS ranking highest by multiple centrality metrics. Receiver operating characteristic analysis confirmed its superior diagnostic performance (AUC = 0.659). Gene set enrichment and correlation analyses demonstrated a robust negative association between FOS expression and multiple mitophagy-related gene sets, including PINK1/Parkin-mediated and receptor-mediated pathways. In TAC mice, FOS was markedly upregulated and accompanied by hypertrophic remodeling, impaired cardiac contractility, elevated p62 accumulation, and reduced LC3-II/LC3-I ratios. In Ang II–treated cardiomyocytes, FOS silencing via siRNA restored mitophagy flux, reduced p62 expression, increased LC3-II conversion, and preserved mitochondrial morphology. FOS is identified as a stress-inducible transcriptional repressor of mitophagy that precipitates mitochondrial dysfunction and maladaptive cardiac remodeling under pressure overload. Mechanistically, hyperactivation of FOS disrupts mitochondrial quality control, triggering oxidative stress, energetic collapse, and subsequent cardiomyocyte loss. Pharmacological or genetic inhibition of FOS reinstates mitophagy and restores mitochondrial homeostasis, thereby attenuating both structural and functional deterioration of the heart. These results delineate a FOS-mitophagy regulatory axis as a mechanistic nexus linking stress signaling to metabolic failure in heart failure, and position FOS as a potential therapeutic target for mechanism-driven, disease-modifying interventions in cardiac hypertrophy and heart failure.

Affiliation:

[1]Department of Cardiology, The First Affiliated Hospital of Soochow University, No. 188 Shizi Street, Suzhou, 215006, China.

[2]The First Affiliated Hospital of Soochow University, No. 188 Shizi Street, Suzhou, 215006, People's Republic of Chia.

***Corresponding author:**
Cao Zou, Department of Cardiology, The First Affiliated Hospital of Soochow University, Suzhou, 215006, China.

Citation: Rui Feng, Meili Liu, Zirui Liu, Haocheng Wang, Danning Cao, Jinghui Ai, Jikai Wang, Weiqi Wang, Cao Zou. FOS-Mediated Mitophagy Suppression Links Stress Signaling to Heart Failure Progression. Cardiology and Cardiovascular Medicine. 10 (2026): 320-332.

Received: April 30, 2026
Accepted: May 05, 2026
Published: June 11, 2026

Feng R, et al., Cardiol Cardiovasc Med 2026
DOI:10.26502/fccm.92920512

Keywords: Heart Failure; FOS; Mitophagy; Mitochondrial Dysfunction; Cardiac Hypertrophy; Transcriptomics.

Introduction

Heart failure (HF) represents the terminal stage of cardiovascular disease, affecting more than 33 million individuals worldwide, with a five-year mortality approaching 53% after diagnosis [1,2]. Although the recently established "quadruple therapy" regimen has markedly improved survival and reduced hospitalization, these treatments primarily target neuroendocrine overactivation and fail to correct the fundamental pathophysiological drivers of HF-namely, myocardial energy depletion and mitochondrial dysfunction [3,4]. The 2025 HFSA/ASPC joint statement underscores that the traditional paradigm of symptom control has reached its therapeutic ceiling, calling for a strategic shift toward preventive and mechanism-based interventions. Central to this transition is the precise targeting of the molecular mechanisms underpinning pathological remodeling and impaired energy metabolism [5]. Among these mechanisms, growing evidence highlights mitochondrial autophagy (mitophagy) imbalance as a pivotal contributor to disease progression. Mitochondria are the metabolic core of cardiomyocytes, and the integrity of their quality-control machinery-particularly mitophagy-directly governs cellular energy homeostasis and survival. Under physiological conditions, moderate mitophagy selectively removes damaged or dysfunctional mitochondria, preserving ATP synthesis and limiting reactive oxygen species (ROS) accumulation to protect cardiomyocytes from oxidative injury. However, as HF advances, mitophagy exhibits a biphasic "double-edged sword" behavior [6]. During the compensatory stage, activation of the canonical PINK1/Parkin pathway enhances mitochondrial clearance, reflected by an increased LC3-II/I ratio and accelerated p62 degradation, thereby delaying cardiac dysfunction [7]. In contrast, during decompensation, mitophagy collapses, leading to p62 accumulation, reduced LC3-II/LC3-I ratio, and the build-up of defective mitochondria [8]. These dysfunctional organelles not only fail to generate ATP efficiently but also become dominant sources of ROS, amplifying oxidative stress and ultimately triggering cardiomyocyte apoptosis and necrosis—hallmarks of progressive HF deterioration [9,10]. The Fos proto-oncogene (FOS), a core component of the immediate-early gene family, plays an essential role in stress adaptation, proliferation, differentiation, and apoptosis [11,12]. In cardiomyocytes, c-Fos is rapidly induced by mechanical stretch, angiotensin II, and oxidative stress, orchestrating transcriptional networks involved in hypertrophy and fibrosis [13]. Sustained c-Fo's activation has been identified as a critical molecular switch driving the transition from compensatory hypertrophy to overt HF [14]. Nevertheless, whether FOS contributes to HF pathogenesis by modulating mitophagy remains largely unexplored. In this study, we integrated three transcriptomic databases (GSE95140, GSE133054, GSE141910) using the Robust Rank Aggregation (RRA) algorithm and batch effect correction to identify differentially expressed genes between HF and normal samples. We then performed GO, KEGG, and PPI analyses to identify core genes, followed by GSEA and GSVA to select significantly enriched pathways. Through vivo and vitro validation, we confirmed the role of these pathways in HF. Our findings provide a novel therapeutic strategy targeting the Fos-mediated mitochondrial autophagy regulatory axis, aimed at improving mitochondrial metabolism in HF and delaying or reversing disease progression.

Methods

GEO datasets and preprocessing

Differential expression analysis was performed using the lima package. Genes with $|\log_2 FC| > 1$ and false discovery rate (FDR) < 0.05 (Benjamini-Hochberg correction) were considered significantly differentially expressed. All results, including normalized expression values, were exported for downstream analysis. Selected DEGs were visualized using heatmaps to illustrate expression clustering patterns, and volcano plots were generated to display the relationship between $\log_2$ fold change and statistical significance. Subsequently, the results were integrated with those obtained from Robust Rank Aggregation (RRA) analysis and data after batch effect correction, and the intersection was taken to derive a final set of robust DEGs.

Functional and pathway enrichment analysis

Functional enrichment analyses were conducted in R to explore the biological significance of the identified genes. Differentially expressed genes were first mapped to Entrez gene identifiers, followed by Gene Ontology (GO) and Kyoto Encyclopedia of Genes and Genomes (KEGG) pathway enrichment analyses using the cluster Profiler package. The resulting enrichment data were visualized as bubble plots to depict the distribution of functional categories and pathway associations, thereby illustrating the potential molecular mechanisms underlying the observed gene expression patterns.

PPI network and hub-gene identification

Significant differentially expressed genes (DEGs) were imported into STRING v11.5 to construct protein-protein interaction (PPI) networks, using a confidence threshold of combined score ≥ 0.7. The resulting network was visualized in Cystoscope v3.x, and functional modules were identified using the MCODE plugin with the following parameters: Degree cutoff = 2, Node score cutoff = 0.2, K-core = 2, and Max depth = 100. To determine key regulatory genes, cyto Hubba was applied to rank nodes according to multiple topological algorithms, including Degree, Betweenness,

Feng R, et al., Cardiol Cardiovasc Med 2026
DOI:10.26502/fccm.92920512

Closeness, Radiality, Bottleneck, MNC, and MCC. The top-ranked genes from each metric were compared, and their intersections were illustrated using an Upset plot, providing a quantitative visualization of gene overlaps across algorithms. This integrative network analysis enabled the identification of robust and biologically meaningful hub genes consistently highlighted by multiple computational criteria.

ROC Analysis and Expression Differential Validation

For each gene, the Receiver operating characteristic (ROC) curve and corresponding area under the curve (AUC) were computed to quantify discriminative performance between groups. Differential expression validation was then performed, and vertical boxplots were generated using the gg boxplot function to visualize group-wise expression patterns. Statistical differences were evaluated with the stat compare means function, and significance levels were denoted as $P < 0.001$ (***), $P < 0.01$ (**), $P < 0.05$. (*), and ns for non-significance.

Gene Set Enrichment Analysis (GSEA)

Gene Set Enrichment Analysis (GSEA) was performed after excluding normal samples to investigate the biological pathways associated with gene expression patterns. Input files were prepared in GCT format, with the second line specifying the number of data rows and processed samples, followed by sample names and gene expression values. The expression level of the FOS gene was extracted, and samples were stratified into high and low expression groups based on the median value. Sample grouping information was saved in a CLS file. The input. CT and input's files were then uploaded into the GSEA software (Broad Institute) for enrichment analysis, and enrichment plots were generated to visualize pathway associations and enrichment trends.

Mitochondrial Autophagy Correlation Analysis

To explore the relationship between target genes and mitochondrial autophagy, eight mitochondrial autophagy–related gene sets (mitochondrial autophagy. gmt) were retrieved from the Molecular Signatures Database (MS ig DB). Single-sample Gene Set Enrichment Analysis (ssGSEA) was performed using the GSVA R package (v1.34.0) to compute enrichment scores for each gene set across all disease samples, and the results were saved as ssgseaOut.txt. Correlations between FOS expression and mitochondrial autophagy enrichment were visualized using a heatmap (gene_expression_FOS.pdf) and line–point plots (FOS_correlation.pdf). These analyses provided insight into the potential regulatory role of FOS in mitochondrial autophagy–related pathways.

Establishment of the TAC Heart Failure Mouse Model

Male C57BL/6J (C57) mice (20–22 g) were obtained from Shanghai SLAC Laboratory Animal Co., Ltd. (Animal License No. SCXK(Shanghai) 2022-0004). All experimental procedures were approved by the Animal Ethics Committee of Soochow University (Approval No. SYSU-IACUC-2020-000469). To establish the transverse aortic constriction (TAC) model, mice were anesthetized with 2% isoflurane and placed in a supine position. Following thoracotomy and exposure of the aortic arch, the aorta was ligated around a 27-gauge needle using a 6-0 silk suture, after which the needle was carefully withdrawn. Sham-operated mice underwent the same surgical procedure without ligation. Postoperatively, animals were extubated, placed on a heating pad to maintain body temperature, and monitored until full recovery from anesthesia [15]. Postoperative analgesia was provided as needed to minimize pain and distress. Animals were monitored daily for general health status and behavior throughout the study period. Humane endpoints were predefined prior to the initiation of the experiment. Mice were euthanized if they exhibited any of the following criteria: (i) body weight loss exceeding 20% of baseline; (ii) severe lethargy or inability to access food or water; (iii) labored or dyspneic breathing; or (iv) other signs of severe distress or poor prognosis as determined by veterinary staff. No animals died unexpectedly before reaching the predefined humane endpoints. All mice were maintained for 4 weeks under standard housing conditions (24 ± 2 °C, 50 ± 10% humidity, 12 h light/dark cycle) with free access to food and water. On day 28 after surgery, mice from both the TAC and sham groups were euthanized by overdose of isoflurane followed by cervical dislocation, in accordance with AVMA Guidelines for the Euthanasia of Animals, and tissues were collected for subsequent analyses.

Echocardiography

Cardiac function was evaluated in both the sham and TAC model groups using a high-resolution Vevo 2100 small-animal ultrasound system (MS400 probe) at baseline (0 weeks) and 4 weeks post-surgery. Left ventricular systolic function was assessed from short-axis M-mode images at the level of the papillary muscles, with measurement of ejection fraction (EF) and fractional shortening (FS). Left ventricular end-diastolic diameter (LVID; d), end-systolic diameter (LVID; s), and posterior wall thickness in diastole and systole (LVPW; d and LVPW; s) were also recorded.

Assessment of Cardiac Index

At the experimental endpoint, mice were euthanized, and hearts were rapidly excised and rinsed in 4 °C saline to eliminate residual blood. After gentle blotting with filter paper, the total heart weight was recorded. The ipsilateral tibia was isolated by removing surrounding soft tissues, and its length was measured from the tibial plateau to the medial malleolus. The heart weight-to-tibia length ratio (HW/TL)

Feng R, et al., Cardiol Cardiovasc Med 2026
DOI:10.26502/fccm.92920512

was calculated as an index of cardiac hypertrophy, providing a standardized morphological parameter for cross-group comparison.

Histological analysis

After completion of the experiment, mouse hearts were immediately exercised and fixed overnight in 4% paraformaldehyde. Following fixation, tissues were embedded in paraffin and sectioned at a thickness of 5 μm. The sections were deparaffinized in xylene and rehydrated through graded ethanol solutions. For histological evaluation, sections were first stained with hematoxylin and eosin (H&E) to assess general myocardial morphology, and subsequently with Masson's trichrome stain to visualize collagen deposition and fibrotic changes within the myocardium.

Primary mouse cardiomyocyte culture and treatment

Primary cardiomyocytes were isolated from neonatal C57BL/6 mice (1-2 days old) following previously described protocols [16]. Briefly, hearts were excised, rinsed in phosphate-buffered saline (PBS), and minced into small fragments. The tissue was enzymatically digested at 37°C in a solution containing trypsin (1.2 mg/mL) and collagenase (0.14 mg/mL). The resulting cell suspensions were collected, and digestion was terminated by adding fetal bovine serum (FBS). Cells were peeled by centrifugation and resuspended in DMEM/F12 medium supplemented with 5% FBS and 0.1 mM bromodeoxyuridine (BrdU) to inhibit fibroblast proliferation. After pre-plating for 1 hour to allow fibroblast attachment, non-adherent cardiomyocytes were transferred to 6-well plates and cultured at 37°C in 5% CO_2 for 48 hours prior to further experiments. Cardiomyocyte hypertrophy was induced by treatment with 1 μM angiotensin II (Ang II) for 24 hours.

Construction of FOS siRNA

The small interfering RNA targeting FOS (si-FOS) was designed and synthesized by Gene Pharma (Suzhou, China). The siRNA sequences were as follows: sense, 5′-GAAGCUGACUCCUUCCCAATT-3′; antisense, 5-UUGGGAAGGAGUCAGCUUCTT-3. Primary mouse cardiomyocytes were seeded into 6-well plates and cultured for 48 hours before transfection. Cells were then transfected with is-FOS using the siRNA-Mate Plus reagent (Gene Pharma, Suzhou, China) according to the manufacturer's protocol. Cardiomyocytes were harvested 48 hours post-transfection for subsequent functional and molecular analyses.

Quantitative real-time PCR (q RT-PCR)

Total RNA was extracted from cardiac tissues and cultured cardiomyocytes using Triazole LS reagent (Invitrogen) following the manufacturer's instructions. RNA concentration and purity were determined using a Nanodrop ND-1000 spectrophotometer. Subsequently, complementary DNA (cDNA) was synthesized with the Go Script™ Reverse Transcription Mix (Promega). Quantitative real-time PCR was performed using the SYBR Green Master Mix (AB clonal) on an Applied Biosystems platform. Relative gene expression levels were calculated using the 2^−ΔΔCt method, with GAPDH serving as the internal control.

Western blot

Total protein was extracted from cardiac tissue and cardiomyocytes using a lysis buffer containing protease inhibitors (Cat. No: P001, NC Biotech), Phosphatase Inhibitor Cocktail (Cat. No: GRF102, Epi Zyme), and RIPA buffer (Cat. No. WB3100, NC Biotech). Protein concentration was determined using the BCA assay. For protein separation, 7.5% (Cat. No: PG121, Epi Zyme), 10% (Cat. No: PG122, Epi Zyme), and 15% (Cat. No: PG124, Epi Zyme) gels were prepared using the Color PAGE Gel Rapid Preparation Kit. Proteins were separated by electrophoresis and transferred to a 0.22 am PVDF membrane. The membrane was blocked with 5% non-fat milk at room temperature for 1 hour and then incubated overnight at 4°C with primary antibodies: BNP (1:1000, Cat. No. A23996, AB clonal), β-MHC (1:2000, Cat. No. 22280-1-AP, Protein tech), FOS (1:5000, Cat. No. 66590-1-Ig, Protein tech), LC3 II/I (1:500, Cat. No. A15591, AB clonal), P62 (1:20000, Cat. No. A19700, AB clonal), and GAPDH (1:25000, Cat. No. 60004-1-Ig, Protein tech). The following day, the membrane was incubated with secondary antibodies: rabbit (1:5000, Cat. No. SA00001-2, Protein tech) or mouse (1:55000, Cat. No. AS003, AB clonal) for 1 hour at room temperature. Signals were detected using ECL (Cat. No. P10060, NCM Biotech), and band intensity was quantified using ImageJ software.

Immunofluorescence staining

For cellular immunofluorescence, primary cardiomyocytes were seeded onto glass coverslips and fixed with 4% paraformaldehyde (PFA) for 15 minutes. After permeabilization with 0.1% Triton X-100 in PBS for 8 minutes, cells were blocked with 1% fetal bovine serum (FBS) for 1 hour at room temperature. Subsequently, cells were incubated overnight at 4°C with a primary antibody against FOS (1:300, CST, Cat. No. 2250). The following day, samples were washed with PBS and incubated for 1 hour at room temperature in the dark with a CoraLite®488-conjugated goat anti-rabbit secondary antibody (1:500, Protein tech, Cat. No. RGAR002). Nuclei were counterstained with DAPI, and fluorescence images were captured using a fluorescence microscope (Nikon). For tissue immunofluorescence, mouse hearts were fixed in 4% paraformaldehyde overnight, embedded in paraffin, and sectioned at 5 μm thickness. After deparaffinization and antigen retrieval, sections were permeabilized with 0.1% Triton X-100, blocked with 5%

Feng R, et al., Cardiol Cardiovasc Med 2026
DOI:10.26502/fccm.92920512

BSA for 1 hour, and incubated overnight at 4°C with primary antibodies against FOS (1:300, CST) and LC3 (1:200, Abcam). The next day, sections were washed and incubated with corresponding Alexa Fluor–conjugated secondary antibodies (1:500, Invitrogen) for 1 hour in the dark. Nuclei were counterstained with DAPI, and fluorescence signals were visualized using a confocal laser scanning microscope (Leica). Images were processed and analyzed using ImageJ software.

Transmission Electron Microscopy (TEM)

Cellular specimens were prepared for ultrastructural analysis by transmission electron microscopy. Briefly, harvested cells were primarily fixed and subsequently immobilized within 1% agarose for handling. Tissue blocks were post-fixed with 1% osmium tetroxide in 0.1 M phosphate buffer (pH 7.4). Following a graded ethanol dehydration series, samples were infiltrated and embedded in EPON-812 resin. Polymerized blocks were sectioned to 70 nm thickness using an ultramicrotome. The sections, mounted on copper grids, were subjected to dual contrast with 2% uranyl acetate and lead citrate before being examined under the microscope [17].

Statistical analysis

Except for bioinformatics data, all quantitative results are presented as mean ± standard error of the mean (SEM). Statistical analyses were performed using GraphPad Prism 10.0 (GraphPad Software, San Diego, USA). Comparisons between two groups were assessed using unpaired, two-tailed Student's *T*-tests. For multiple group comparisons, one-way or two-way analysis of variance (ANOVA; when two factors were involved) was applied, followed by Bonferroni's post hoc test for multiple comparisons. Statistical significance was defined as $P < 0.05$.

Results

Identification of DEGs in HF Samples compared with Not-Failing Samples

Transcriptomic profiling of the GSE95140, GSE133054, and GSE141910 datasets revealed distinct gene expression patterns between heart failure (HF) and non-failing (NF) or control hearts. In the GSE95140 dataset, 546 differentially expressed genes (DEGs) were identified, including 116 upregulated and 430 downregulated genes (P<0.05, |fold change|>2) (figure 1A). The SE133054 dataset yielded 1,243 DEGs (686 upregulated, 557 downregulated) (figure 1b), while analysis of GSE141910 identified 196 DEGs (109 upregulated, 87 downregulated) (figure 1c). To integrate these independent datasets, we applied the Robust Rank Aggregation (RRA) method (Figure 1d) in combination with batch-effect correction (figure 1e), followed by intersection analysis to identify consistently dysregulated genes across cohorts (figure 1f). This integrative approach reduced dataset bias and facilitated the identification of robust HF-associated transcriptional signatures.

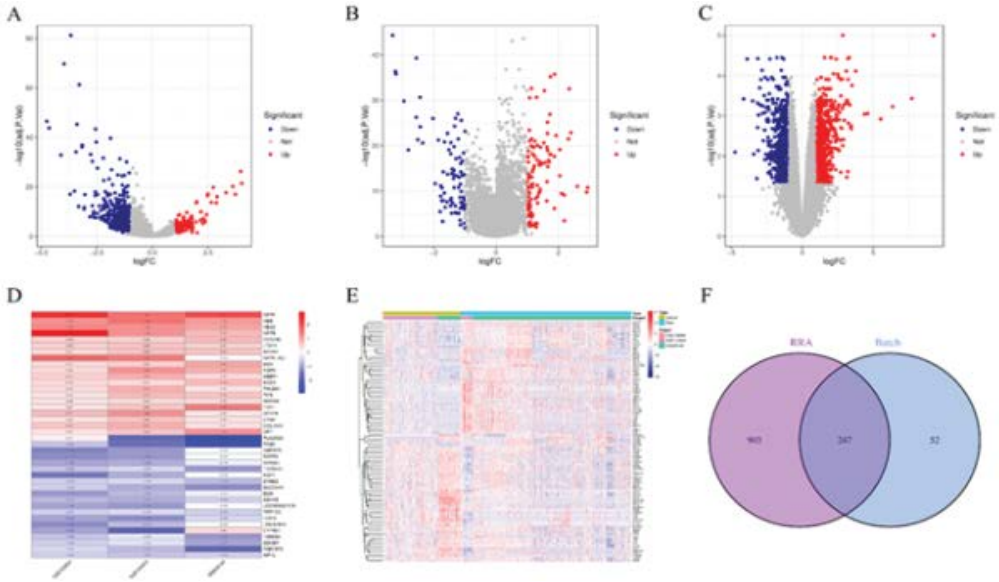


Figure 1: Identification and integrative analysis of differentially expressed genes across three GEO datasets. (A-C) Volcano plots illustrating differentially expressed genes (DEGs) in the GSE95140, GSE133054, and GSE141910 datasets, respectively. Red dots represent significantly upregulated genes, blue dots indicate significantly downregulated genes, and grey dots denote nonsignificant genes. (D) Heatmap showing expression patterns of DEGs identified by robust rank aggregation (RRA) analysis. (E) Heatmap showing gene expression profiles after batch-effect correction, indicating improved consistency across datasets. (F) Venn diagram illustrates the overlap between DEGs identified by the RRA and batch-corrected analyses; the intersection represents genes consistently detected by both methods.

Feng R, et al., Cardiol Cardiovasc Med 2026
DOI:10.26502/fccm.92920512

Functional enrichment analysis of differentially expressed genes

Functional enrichment analysis of the 247 DEGs was conducted using GO and KEGG frameworks to elucidate their potential biological roles. GO analysis revealed that the DEGs were significantly enriched in oxidative phosphorylation, mitochondrial ATP synthesis coupled with electron transport, and ATP metabolic process within the biological process (BP) category (figure 2a). In the cellular component (CC) category, these genes were mainly localized to the mitochondrial respirasome, respiratory chain complex, and mitochondrial inner membrane (figure 2b). Molecular function (MF) enrichment indicated significant involvement in NADH dehydrogenase activity and electron transfer activity (figure 2c). Consistently, KEGG pathway analysis identified oxidative phosphorylation, diabetic cardiomyopathy, and non-alcoholic fatty liver disease as the most significantly enriched pathways (figure 2d). Together, these findings underscore the central role of mitochondrial dysfunction and impaired energy metabolism in the pathogenesis of heart failure.

PPI network analysis

PPI network of 247 DEGs was constructed using the STRING database, comprising 50 nodes and 286 edges (Fig. 3A). Network topology was further analyzed in Cytoscope. Significant gene clusters were identified using the MCODE plugin (default parameters: degree cutoff = 2, node score cutoff = 0.2, k-core = 2, max depth = 100). The highest-scoring module, consisting of 15 nodes and 93 edges, was defined as the key cluster (Fig. 3B), encompassing genes such as NPPA, TAGLN, B2M, NPPB, AQP1, CCL2, TNN3, EGR1, CDH5, LTBP2, APOA1, ENG, MMP2, and FOS. To identify hub genes, we ranked the top ten nodes based on multiple centrality measures, including MCC, betweenness, radiality, closeness, bottleneck, degree, and maximum neighborhood component (MNC) (Fig. 3C). Intersection analysis of these metrics revealed five hub genes FOS, VWF, TAGLN, B2M, and CCL2 which may play pivotal roles in the molecular network.

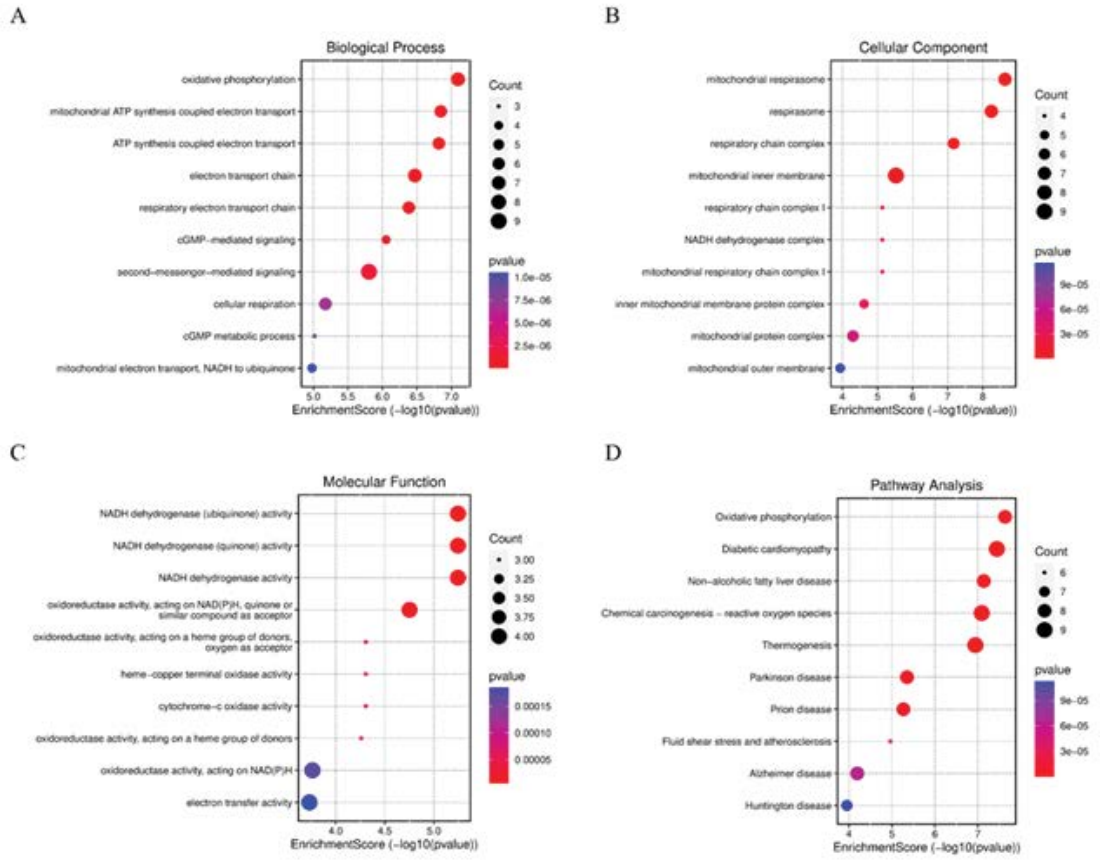


Figure 2: Functional enrichment analysis of the intersecting genes. (A-C) GO enrichment analysis classified into BP, CC and MF categories. The plots display the top enriched GO terms ranked by statistical significance. (D) KEGG pathway enrichment analysis showing the top enriched signaling pathways.

Citation: Rui Feng, Meili Liu, Zirui Liu, Haocheng Wang, Danning Cao, Jinghui Ai, Jikai Wang, Weiqi Wang, Cao Zou. FOS-Mediated Mitophagy Suppression Links Stress Signaling to Heart Failure Progression. Cardiology and Cardiovascular Medicine.10 (2026): 320-332.

Feng R, et al., Cardiol Cardiovasc Med 2026
DOI:10.26502/fccm.92920512

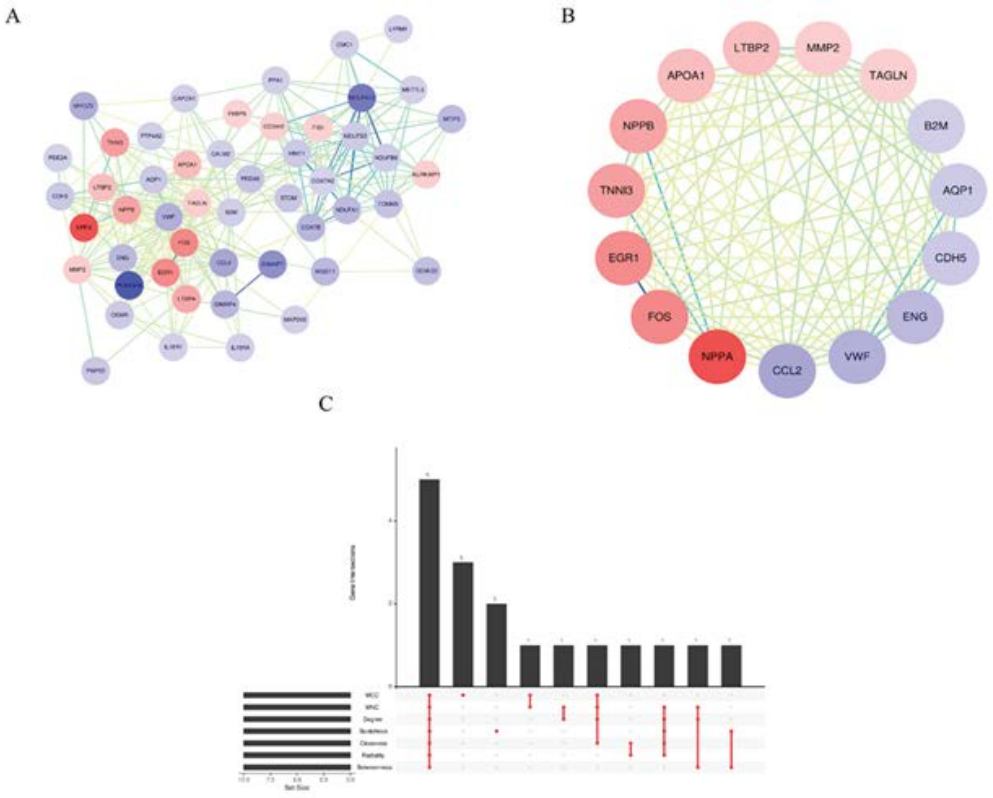


Figure 3: PPI network analysis of shared DEGs. (A) PPI network of shared DEGs constructed in the STRING database. (B) Interaction network showing DEG relationships, with node colors denoting expression patterns (red, upregulated; blue, downregulated). (C) Hub genes identified based on multiple topological scoring algorithms, highlighting VWF, TAGLN, CCL2, FOS, and B2M as key central nodes within the network.

Hub-gene ROC analysis identifies FOS as a key marker inversely associated with mitophagy

ROC analysis of the five overlapping genes (B2M, FOS, CCL2, TAGLN, and VWF) revealed that all exhibited AUC values above 0.5, suggesting potential diagnostic relevance in distinguishing Control and Treat groups. Among these, FOS showed the highest AUC (0.659), indicating the strongest discriminatory power, followed by VWF (0.631) and CCL2 (0.620), whereas B2M (0.575) and TAGLN (0.574) displayed modest but above-chance AUCs (Fig. 4A). Consistently, boxplot analysis showed significantly different expression levels of these genes between groups, further supporting their diagnostic potential (Fig. 4B).To explore the biological relevance of FOS, GSEA based on FOS expression (median split) revealed significant enrichment of the mitophagy pathway (REACTOME_MITOPHAGY; normalized enrichment score [NES] = 1.99, nominal $P < 0.001$, FDR $q = 0.002$, FWER $P = 0.023$; Fig. 4C), meeting the predefined significance threshold (FDR $q < 0.05$).Correlation analyses further confirmed consistent negative associations between FOS expression and multiple mitophagy-related gene sets, including GOBP_MITOPHAGY ($r = -0.29$, $P = 3.6\times10^{-11}$), REACTOME_MITOPHAGY ($r = -0.28$, $P = 2.0\times10^{-10}$), and REACTOME_PINK1_PRKN_MEDIATED_MITOPHAGY ($r = -0.26$, $P = 8.1\times10^{-9}$), among others ($|r| = 0.24$–0.29, $P < 1\times10^{-7}$). Smaller yet significant correlations were also observed for REACTOME_RECEPTOR_MEDIATED_MITOPHAGY ($r=-0.15$,$P=0.0012$) and GOBP_POSITIVE_REGULATION_OF_MITOPHAGY_IN_RESPONSE_TO_MITOCHONDRIAL_DEPOLARIZATION ($r = -0.12$, $P = 0.0082$).Collectively, these data demonstrate a robust inverse relationship between FOS expression and multiple mitophagy pathways—including PINK1–PRKN-mediated, receptor-mediated, and regulatory modules—suggesting that elevated FOS levels are associated with reduced mitophagy activity (Fig. 4D–J).

FOS is markedly upregulated in pressure overload–induced cardiac hypertrophy to investigate

The role of FOS in pressure overload–induced cardiac remodeling and dysfunction, we generated a TAC mouse model and comprehensively evaluated cardiac structure and function. Echocardiography revealed a pronounced decline in contractile performance in TAC mice, evidenced by a significant reduction in left EF, FS LVIDd, LVIDs, LVPWD and LVPWS compared with sham-operated controls ($P < 0.05$; Figure. 5A-H). Consistent with these

Feng R, et al., Cardiol Cardiovasc Med 2026
DOI:10.26502/fccm.92920512

findings, post-mortem morphometry showed marked increases in both HW/BW and HW/TL ratios in the TAC group ($P < 0.05$; Figure. 5E, F), confirming the development of pathological hypertrophy. Histological analysis further supported these observations. H&E staining demonstrated enlarged cardiomyocyte cross-sectional areas in TAC hearts ($P < 0.05$; Figure. 6A), while molecular assays revealed robust activation of hypertrophic markers. Quantitative RT–PCR and Western blotting showed a significant upregulation of BNP in TAC hearts relative to sham controls ($P < 0.05$; Figure. 6B). Notably, FOS expression was strongly elevated at both the mRNA and protein levels in TAC-induced myocardium ($P < 0.05$; Figure. 6C, D). Immunofluorescence imaging corroborated these molecular results, showing markedly increased FOS fluorescence intensity in TAC cardiac tissues ($P < 0.05$; Figure. 6E, F). These results provide converging evidence that pressure overload elicits robust FOS induction in the myocardium, coinciding with the onset of cardiac hypertrophy and functional decline. This coordinated upregulation implicates FOS as a potential transcriptional regulator driving maladaptive cardiac remodeling under chronic mechanical stress.

FOS knockdown restores mitophagy and preserves mitochondrial integrity in Ang II–induced cardiomyocyte remodeling

To delineate the role of FOS in pathological cardiomyocyte remodeling, primary mouse cardiomyocytes were exposed to 1 μM Ang II for 24 hours to establish an in vitro model of heart failure, followed by targeted FOS

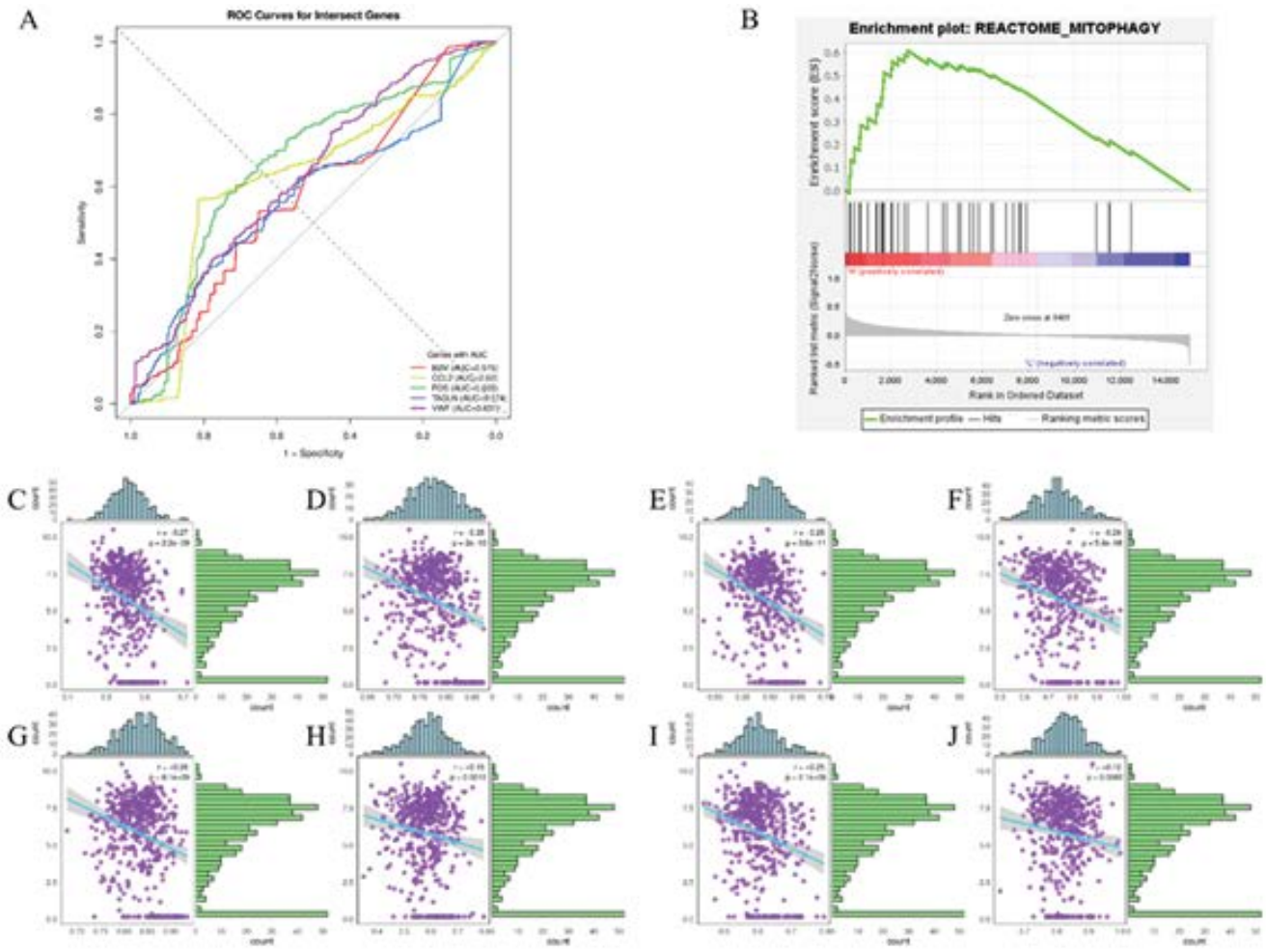


Figure 4: Diagnostic performance of candidate genes and the association between FOS expression and mitophagy activity.(A) ROC analysis highlighted FOS as the most diagnostically informative gene.(B) When samples were stratified by FOS expression, GSEA demonstrated a significant enrichment of the mitophagy pathway (REACTOME_MITOPHAGY), comprising 36 genes (NES = 1.99, NOM $P < 0.001$, FDR $q = 0.002$, FWER $P = 0.023$), satisfying the significance criterion of FDR $q < 0.05$. This indicates a tight association between FOS expression and mitophagy pathway activity. (C-J) In line with these results, GSVA enrichment analysis of mitophagy-related gene sets suggested that FOS acts as a transcriptional suppressor, negatively regulating mitophagy-associated signaling.

Citation: Rui Feng, Meili Liu, Zirui Liu, Haocheng Wang, Danning Cao, Jinghui Ai, Jikai Wang, Weiqi Wang, Cao Zou. FOS-Mediated Mitophagy Suppression Links Stress Signaling to Heart Failure Progression. Cardiology and Cardiovascular Medicine.10 (2026): 320-332.

Feng R, et al., Cardiol Cardiovasc Med 2026
DOI:10.26502/fccm.92920512

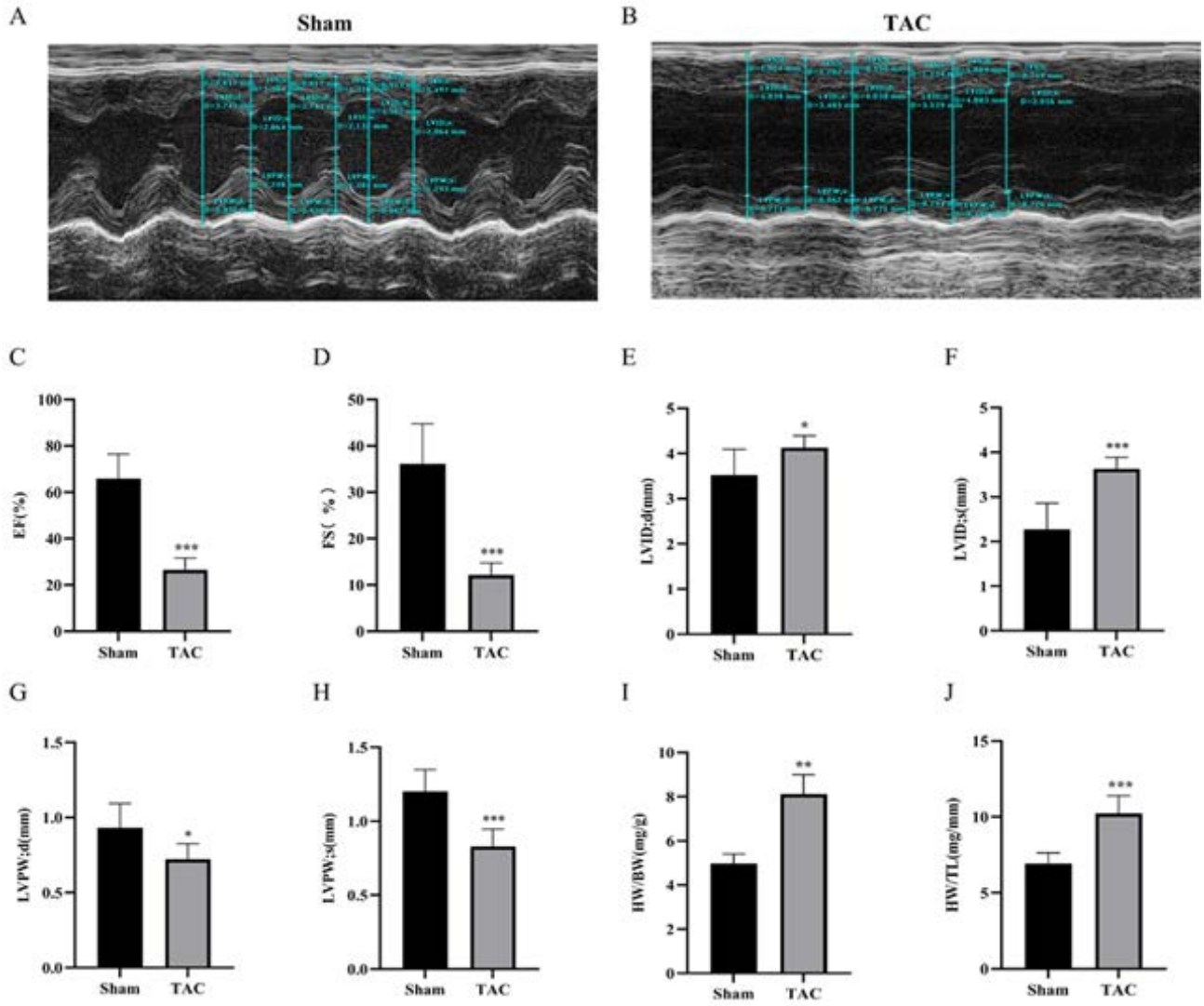


Figure 5: Echocardiographic and morphological evidence of cardiac hypertrophy in TAC-induced mice. (A, B) Representative M-mode echocardiographic images of sham and TAC mice at 4 weeks post-surgery. (C-H) EF, FS, LVIDd, LVIDs, LVPWD and LVPWS obtained from echocardiography (n = 6 per group). (I, J) Morphometric assessment showing increased HW/BW and HW/TL ratios in TAC mice compared with sham controls (n = 6 per group).

knockdown. The successful induction of hypertrophic stress and efficient FOS silencing were confirmed at the protein, transcript, and immunofluorescence levels (Figure. 7A-E). Ang II stimulation markedly increased the expression of the hypertrophic and stress markers BNP and FOS, whereas FOS silencing effectively reversed these changes, underscoring the regulatory role of FOS in Ang II–induced cardiomyocyte remodeling. To determine whether FOS modulates this process through the mitophagy pathway, we examined the autophagy markers p62 and LC3-I/II. Ang II exposure significantly suppressed mitophagy activity, evidenced by p62 accumulation and a decreased LC3-II/LC3-I ratio (Fig. 7A, B). In contrast, FOS knockdown restored autophagic flux, suggesting that elevated FOS levels inhibit mitophagy under pathological stress. Consistent with these molecular findings, TEM provided ultrastructural confirmation: cardiomyocytes treated with Ang II displayed pronounced mitochondrial swelling and disrupted cristae, whereas FOS silencing partially preserved mitochondrial morphology and increased the number of autophagosomes (Fig. 7F). Collectively, these data demonstrate that FOS is strongly induced under cardiomyocyte stress, where its upregulation suppresses mitophagy, leading to mitochondrial dysfunction and structural injury. Conversely, FOS inhibition reactivates mitophagy, restores mitochondrial homeostasis, and mitigates cellular damage, identifying FOS as a key transcriptional regulator of mitochondrial quality control in cardiac stress responses.

Feng R, et al., Cardiol Cardiovasc Med 2026
DOI:10.26502/fccm.92920512

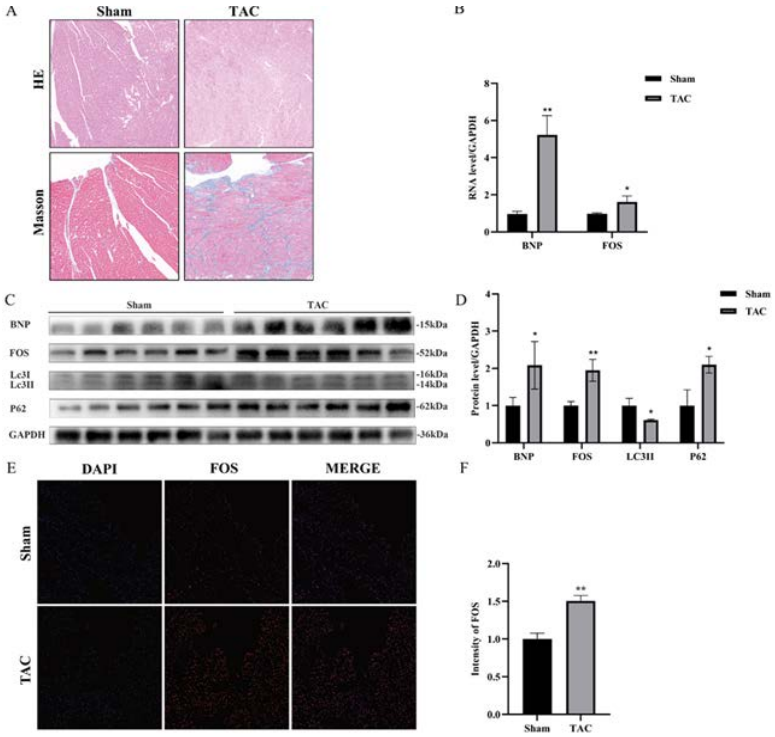


Figure 6: Histological and molecular validation of FOS upregulation and altered autophagy in TAC-induced cardiac hypertrophy.(A) Representative H&E and Masson's trichrome staining of left ventricular cross-sections from sham and TAC-operated mice at 4 weeks post-surgery.(B) Relative mRNA expression levels of BNP and FOS in cardiac tissues from sham and TAC groups.(C,D) Protein expression and quantification of BNP, FOS, and autophagy-related markers LC3 and P62 in heart tissues.(E) Representative immunofluorescence staining and quantification of FOS expression in cardiac tissue sections.

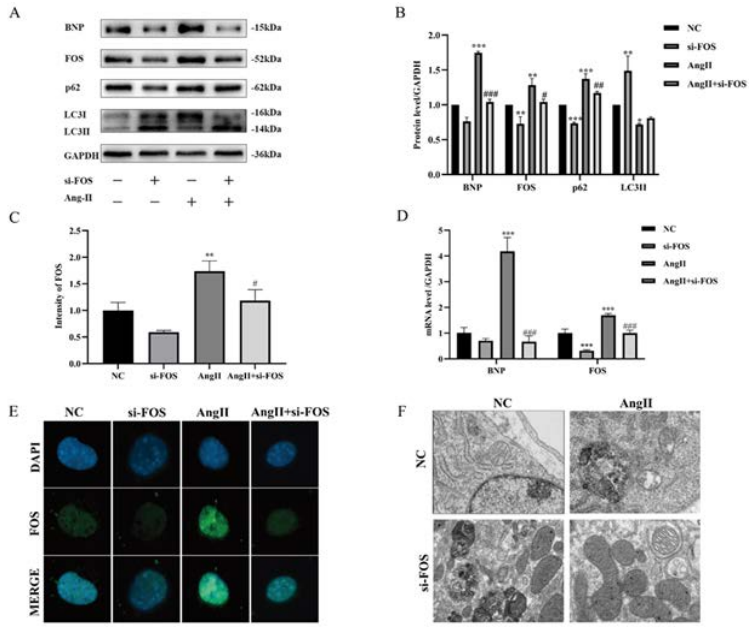


Figure 7: FOS expression and autophagy alterations in primary cardiomyocytes isolated from TAC mice.(A,B) Western blot analysis and quantification of BNP, FOS, and autophagy-related markers LC3 and P62 in primary cardiomyocytes from sham and TAC groups.(C,E) Representative immunofluorescence staining and quantification of FOS expression in primary cardiomyocytes.(D) Relative mRNA expression levels of BNP and FOS in primary cardiomyocytes from each group.(F) Representative TEM images showing ultrastructural changes in cardiomyocytes from sham and TAC mice.

Citation: Rui Feng, Meili Liu, Zirui Liu, Haocheng Wang, Danning Cao, Jinghui Ai, Jikai Wang, Weiqi Wang, Cao Zou. FOS-Mediated Mitophagy Suppression Links Stress Signaling to Heart Failure Progression. Cardiology and Cardiovascular Medicine.10 (2026): 320-332.

Feng R, et al., Cardiol Cardiovasc Med 2026
DOI:10.26502/fccm.92920512

Discussion

HF remains a leading global cause of death and disability, with incidence rising alongside population ageing and persistently poor long-term survival [18]. Its complex pathogenesis involves myocardial injury, neuroendocrine overactivation, ventricular remodeling, and metabolic impairment [19]. Mitochondrial dysfunction—including impaired oxidative phosphorylation, oxidative stress, and abnormal dynamics—has emerged as a key driver of metabolic failure and HF progression [20,21]. Mitophagy, the selective degradation of damaged mitochondria, is essential for maintaining cardiomyocyte energy homeostasis: moderate activation is protective, while dysregulation accelerates cell death [22,23]. However, the upstream regulatory networks that tune mitophagy during HF-particularly how stress-responsive transcriptional programs control this process-remain largely undefined. Among these regulators, the Fos/AP-1 pathway serves as a central immediate-early response system. FOS, activated by diverse stimulus such as pressure overload, ischemia, or inflammation, forms heterodimers with Jun family proteins to create the AP-1 complex, which governs genes involved in proliferation, apoptosis, and fibrosis [24-26]. Aberrant c-Fo's expression has been linked to myocarditis, dilated cardiomyopathy, and ischemia–reperfusion injury, where AP-1 drives apoptosis and matrix remodeling [27,28]. Despite extensive study, its precise role in HF protective or pathogenic-has remained unresolved. Here, by integrating transcriptomic data from three independent HF cohorts, we identified FOS as a hub gene negatively correlated with mitophagy activity, suggesting its involvement as a transcriptional suppressor in mitochondrial quality control. Our experimental validation supports this model. In TAC-induced HF mice, FOS upregulation paralleled contractile dysfunction, ventricular hypertrophy, and fibrosis, accompanied by p62 accumulation and reduced LC3-II/LC3-I ratios, indicating mitophagy failure. Similar changes were observed in Ang II–treated cardiomyocytes, confirming the consistency across in vivo and in vitro systems. Mechanistically, siRNA-mediated FOS knockdown restored autophagic flux, reduced p62 levels, increased LC3-II conversion, preserved mitochondrial structure, and lowered hypertrophic markers such as BNP and MYH7. These findings demonstrate that excessive FOS activation suppresses mitophagy, exacerbating mitochondrial dysfunction and accelerating HF progression, whereas its inhibition reinstates mitochondrial homeostasis and mitigates pathological remodeling. Collectively, this work positions FOS as a key pathological amplifier that couples stress signaling mitochondrial dysfunction. Persistent FOS overexpression represses mitophagy, promotes ROS accumulation and energy crisis, and drives cardiomyocyte death, forming a self-reinforcing loop of metabolic failure and remodeling. Conversely, FOS inhibition interrupts this cycle and restores energetic balance. We thus define a FOS–mitophagy axis that bridges metabolic derangement and structural remodeling, offering a dual-benefit therapeutic target. Future studies should delineate the precise mechanisms of FOS-dependent mitophagy repression and develop cardiomyocyte-selective FOS modulators, such as PROTAC-based degraders or AAV/ASO-mediated silencing. These strategies could enable mechanism-based, disease-modifying interventions-aligning with the HFSA/ASPC vision of transforming HF therapy from symptom control to causal correction.

Conclusion

This study identifies FOS as a pivotal transcriptional repressor of mitophagy in pressure overload–induced heart failure. These findings uncover a previously unrecognized FOS mitophagy axis that mechanistically connects stress signaling to metabolic failure in heart failure, highlighting FOS as a potential therapeutic target for mechanism-based intervention in this disease.

Acknowledgments: Not applicable.

Author Contributions

Rui Feng and Meili Liu conceived and designed the study, and drafted the manuscript., Zirui Liu, Haocheng Wang, Danning Cao and Jinghui Ai, performed the experiments and collected the data. Jikai Wang and Weiqi Wang analyzed the data and organized the results. Cao Zou supervised the study, revised the manuscript, and provided funding support. All authors have read and approved the final version of the manuscript.

Declaration of conflicting interests

The authors declare that they have no known competing financial interests or personal relationships that could have appeared to influence the work reported in this paper.

Ethical Approval

The animal experiments conformed to the Guide for the Care and Use of Laboratory Animals. Animal study has been approved by the Animal Ethics Committee of Ethics Committee of Soochow University.

Clinical trial numbers: Not applicable.

Informed Consent: All animal studies comply with the ARRIVE guidelines.

Funding

The study was supported by the Suzhou Science and Technology Project (SKYD2022103), Jiangsu Commission of Health (K2023080) and Soochow University (P112206422).

Data availability statement

The datasets generated and/or analyzed during the current study are available from the corresponding author, Dr. Cao Zou, upon reasonable request (Email: nkzc75@suda.edu.cn).

References

1. Beghini A, Sammartino AM, Papp Z, et al. 2024 update in heart failure. ESC Heart Fail 12 (2025): 08-42.
2. Tomasoni D, Adamo M, Lombardi CM, et al. Highlights in heart failure. ESC Heart Fail 6 (2019): 1105-1127.
3. Zhao D, Zhang Y, Yong Y, et al. Vericiguat combined with "new quadruple" therapy enhances cardiac function and life quality in patients with heart failure: a single-center prospective study. Front Cardiovasc Med 11 (2024): 1476976.
4. Jin N, Zhang M, Zhou L, et al. Mitochondria transplantation alleviates cardiomyocytes apoptosis through inhibiting AMPKα-mTOR mediated excessive autophagy. Faseb j 38 (2024): e23655.
5. Zhou H, He L, Xu G, et al. Mitophagy in cardiovascular disease. Clin Chim Acta 507 (2020): 210-218.
6. Fu J, Su C, Ge Y, et al. PDE4D inhibition ameliorates cardiac hypertrophy and heart failure by activating mitophagy. Redox Biol 81 (2025): 103563.
7. Miranda-Silva D, P G.R, Alves E, et al. Mitochondrial Reversible Changes Determine Diastolic Function Adaptations During Myocardial (Reverse) Remodeling. Circ Heart Fail 13 (2020): e006170.
8. Zhou H, Wang X, Xu T, et al. PINK1-mediated mitophagy attenuates pathological cardiac hypertrophy by suppressing the mtDNA release-activated cGAS-STING pathway. Cardiovasc Res 121 (2025): 128-142.
9. Xia G, Xu J, Chen M, et al. Loss of ALDH2 aggravates mitochondrial biogenesis disorder in cardiac myocytes induced by TAC. Biochem Biophys Res Commun 639 (2023): 189-196.
10. Oka T, Hikoso S, Yamaguchi O, et al. Mitochondrial DNA that escapes from autophagy causes inflammation and heart failure. Nature 485 (2012): 251-255.
11. Zhuang L, Wang Y, Chen Z, et al. Global Characteristics and Dynamics of Single Immune Cells After Myocardial Infarction. J Am Heart Assoc 11 (2022): e027228.
12. Jing Y, Zheng W, Zhou Z, et al. Recent research shows advances of c-fos in regulating cell senescence. Arch Biochem Biophys 769 (2025): 110423.
13. Palomer X, Román-Azcona M.S, Pizarro-Delgado J, et al. SIRT3-mediated inhibition of FOS through histone H3 deacetylation prevents cardiac fibrosis and inflammation. Signal Transduct Target Ther 5 (2020): 14.
14. Fan S, Xiao G, Ni J, et al. Guanxinning injection ameliorates cardiac remodeling in HF mouse and 3D heart spheroid models via p38/FOS/MMP1-mediated inhibition of myocardial hypertrophy and fibrosis. Biomed Pharmacother 162 (2023): 114642.
15. Ye B, Zhou H, Chen Y, et al. USP25 Ameliorates Pathological Cardiac Hypertrophy by Stabilizing SERCA2a in Cardiomyocytes. Circ Res 132 (2023): 465-480.
16. Ju J, Wang K, Liu F, et al. Crotonylation of NAE1 Modulates Cardiac Hypertrophy via Gelsolin Neddylation. Circ Res 135 (2024): 806-821.
17. Yoshii A, McMillen T.S, Wang Y, et al. Blunted Cardiac Mitophagy in Response to Metabolic Stress Contributes to HFpEF. Circ Res 135 (2024): 1004-1017.
18. Martin SS, Aday AW, Almarzooq ZI, et al. 2024 heart disease and Stroke Statistics: A Report of US and Global Data from the American Heart Association. Circulation 149 (2024): e347-e913.
19. Adamo M, Chioncel O, Pagnesi M, et al. Epidemiology, pathophysiology, diagnosis and management of chronic right-sided heart failure and tricuspid regurgitation. A clinical consensus statement of the Heart Failure Association (HFA) and the European Association of Percutaneous Cardiovascular Interventions (EAPCI) of the ESC. Eur J Heart Fail 26 (2024): 18-33.
20. Gallo G, Rubattu S, Volpe M. Mitochondrial Dysfunction in Heart Failure: From Pathophysiological Mechanisms to Therapeutic Opportunities. Int J Mol Sci 25 (2024): 2667.
21. Hinton A, Claypool SM, Neikirk K, et al. Mitochondrial Structure and Function in Human Heart Failure. Circ Res 135 (2024): 372-396.
22. Ajoolabady A, Chiong M, Lavandero S, et al. Mitophagy in cardiovascular diseases: molecular mechanisms, pathogenesis, and treatment. Trends Mol Med 28 (2022): 836-849,
23. Yan M, Gao J, Lan M, et al. DEAD-box helicase 17 (DDX17) protects cardiac function by promoting mitochondrial homeostasis in heart failure. Signal Transduct Target Ther 9 (2024): 127.
24. Ti Y, Hao MX, Li CB, et al. Rosiglitazone attenuates myocardial remodeling in spontaneously hypertensive rats. Hypertens Res 34 (2011): 354-360.
25. Wei SG, Yu Y, Zhang ZH, et al. Mitogen-activated protein

Feng R, et al., Cardiol Cardiovasc Med 2026
DOI:10.26502/fccm.92920512

kinases mediate upregulation of hypothalamic angiotensin II type 1 receptors in heart failure rats. Hypertension 52 (2008): 679-686.

26. Min W, Bin ZW, Quan ZB, et al. The signal transduction pathway of PKC/NF-kappa B/c-fos may be involved in the influence of high glucose on the cardiomyocytes of neonatal rats. Cardiovasc Diabetol 8 (2009): 8.

27. Schlieper A, Anwar M, Heger J, et al. Repression of anti-apoptotic genes via AP-1 as a mechanism of apoptosis induction in ventricular cardiomyocytes. Pflugers Arch 454 (2007): 53-61.

28. Bergman M R, Cheng S, Honbo N, et al. A functional activating protein 1 (AP-1) site regulates matrix metalloproteinase 2 (MMP-2) transcription by cardiac cells through interactions with JunB-Fra1 and JunB-FosB heterodimers. Biochem J 369 (2003): 485-496.

This article is an open access article distributed under the terms and conditions of the Creative Commons Attribution (CC-BY) license 4.0

Citation: Rui Feng, Meili Liu, Zirui Liu, Haocheng Wang, Danning Cao, Jinghui Ai, Jikai Wang, Weiqi Wang, Cao Zou. FOS-Mediated Mitophagy Suppression Links Stress Signaling to Heart Failure Progression. Cardiology and Cardiovascular Medicine.10 (2026): 320-332.